Adaptive distributed-feedback semiconductor laser

Chaoze Zhang,[1,*] Tianyu Guan,[1,*] Ligang Huang,[1,†] Yujia Li,[1] Laiyang Dang,[2] Yuqin Mao,[1] Lei Gao,[1] Leilei Shi,[1] Guolu Yin,[1] Chaoyang Gong,[1] and Tao Zhu[1,‡]

[1]*Key Laboratory of Optoelectronic Technology and Systems (Ministry of Education), Chongqing University, Chongqing 400044, China*

[2]*Photonics Research Institute, Department of Electrical and Electronic Engineering, The Hong Kong Polytechnic University, Hong Kong, China*

(Received 10 May 2024; revised 21 March 2025; accepted 27 March 2025; published 9 April 2025)

To solve the difficulty in wavelength adaptability of external-cavity semiconductor lasers, external-cavity distributed feedback has been proven to be an effective method to achieve adaptive narrow-linewidth semiconductor lasers. For the structural design and precise manufacturing of adaptive semiconductor lasers, the principle of laser linewidth compression based on distributed feedback needs to be explored. In this article, we propose a theoretical model for analyzing the operational mechanism of the adaptive distributed-feedback semiconductor laser. Theoretical and experimental results show that achieving adaptive linewidth compression requires tens of or more feedback points. On the basis of sufficient feedback points, increasing the feedback length and ratio can achieve an ultranarrow laser linewidth and high side-mode suppression ratio. This work provides a model analysis tool for exploring the ideal configuration of adaptive narrow-linewidth semiconductor lasers, which paves the way for the design and manufacturing of high-performance semiconductor lasers.

DOI: 10.1103/PhysRevA.111.043511

I. INTRODUCTION

In recent years, there has been a growing demand for high-performance narrow-linewidth semiconductor lasers, driven by their crucial applications in cold-atomic physics [1–5], gravitational wave detection [6–10], cavity electrodynamics [11–14], coherent optical communication [15,16], ultraprecision measurement [17–19] and so on. The external-cavity feedback laser is a promising platform for achieving a high-performance semiconductor laser with a narrow linewidth and high side-mode suppression ratio (SMSR). In order to meet the precision tuning requirement of the narrow-linewidth laser in its applications, the external-cavity semiconductor laser needs to gain wavelength-adaptive ability to output narrow-linewidth laser at any wavelength.

In the field of narrow-linewidth semiconductor lasers, single (few) external-cavity feedback configurations can achieve narrow linewidths [20–23]. However, such typical external feedback will cause laser phase mutation and induce the laser to oscillate with multiple new longitudinal modes under certain conditions, which cannot achieve the wavelength-adaptive output of the external-cavity feedback laser. To suppress the side-longitudinal modes introduced by the external cavity, frequency-selective resonant external cavities are utilized to compress the linewidth of semiconductor laser [23–35], such as fiber (waveguide) Bragg gratings, whispering-gallery mode microcavities, Fabry-Pérot cavities, and so on. Resonant feedback with high Q can deeply compress the laser linewidth and maintain a high SMSR. However, it is necessary to lock the laser wavelength of the main cavity at the resonant wavelength of the feedback cavity, and it is difficult to obtain wavelength-adaptive laser output just through tuning the main cavity. Moreover, when the resonant wavelength of the external cavity fluctuates due to thermal noise or acoustic vibration caused by the surrounding environment, the external-cavity laser is prone to lost locking, making it difficult to maintain narrow-linewidth operation for a long time, especially under industrial conditions.

To overcome the constraints of the single (few) and resonant external-cavity feedback, in 2010 we proposed a narrow-linewidth laser model assisted by the external-cavity distributed feedback that utilizes Rayleigh scattering [36–39]. In 2014, the distributed-feedback structure was utilized to compress the linewidth of a fiber laser to 130 Hz [40]. The distributed-feedback mechanism was further applied to tunable lasers and accomplished the simultaneous linewidth compression of different wavelength [41–44]. Integrated distributed-feedback lasers have also been shown to narrow the linewidth to 10 Hz with distributed feedback, and can also achieve adaptive linewidth compression after wavelength switching, which is attributed to the wide and uniform spectral characteristics of the scattering spectrum after multiple points [45]. Experimentally, a linewidth as narrow as 435 Hz has been achieved in a vertical-cavity surface-emitting laser (VCSEL) with distributed feedback [46]. Distributed feedback has also been demonstrated to be used for linewidth compression of a multiwavelength laser array with an arbitrary wavelength spacing [47]. This further demonstrates the wavelength-adaptive characteristics of Rayleigh scattering under multiwavelength conditions. In addition, distributed feedback can also be utilized in random lasers to achieve narrow-linewidth lasers on the kilohertz level [48–57].

*These authors contributed equally to this work.
†Contact author: lghuang@cqu.edu.cn
‡Contact author: zhutao@cqu.edu.cn

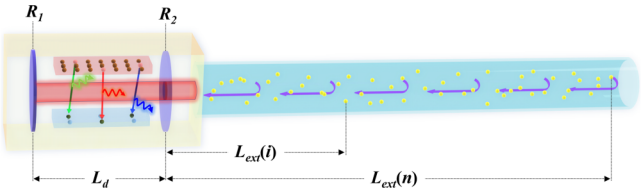

FIG. 1. Schematic diagram of adaptive distributed-feedback laser.

Although external-cavity distributed feedback has demonstrated excellent adaptive linewidth compression characteristics, long fibers are not beneficial for on-chip integration of external-cavity semiconductor lasers. To precisely design the distributed-feedback structure, the quantity of feedback points, the length of the feedback cavity, and the feedback ratio are critical parameters. In previous studies, the qualitative exploration of feedback quantity, feedback cavity length, and feedback ratio has not been addressed. These uncertainties in parameters increase the difficulty of finely designing distributed-feedback structures, necessitating further discussion on the linewidth-compression principles of distributed feedback.

In this article, we propose a mathematical model to describe adaptive distributed-feedback semiconductor lasers. Based on the proposed theoretical model, we analyze the effects of the quantity of feedback points, the length of the feedback cavity, and the feedback ratio on the laser linewidth and SMSR. As the quantity of feedback points, the length of the feedback cavity, and the feedback ratio increase, the laser linewidth becomes narrower, and the SMSR becomes higher. It is worth noting that achieving adaptive linewidth compression only requires tens of, or more, feedback points. Additionally, the stability of external-cavity distributed feedback is theoretically investigated. We further construct a laser system with 10 distributed feedback points. Experimental results demonstrate that the external-cavity distributed feedback can achieve narrow-linewidth compression of around 400 Hz while maintaining high SMSR, confirming good consistency between theoretical predictions and experimental observations. This work provides a model analysis tool for exploring the ideal configuration of adaptive narrow-linewidth semiconductor lasers, paving the way for the design and manufacture of high-performance semiconductor lasers.

II. THEORY AND NUMERICAL SIMULATION

We propose a theoretical model of calculating adaptive distributed-feedback semiconductor lasers, as shown in Fig. 1. The structure consists of a single longitudinal model main-cavity laser and a set of randomly distributed feedback points, each with the same feedback ratio. The distance between each feedback and the output mirror of the main-cavity laser is $L_{\text{ext}}(i)$. On the basis of the single-cavity feedback laser model at medium-feedback level by Schunk *et al.* [58,59], we can further derive the laser rate equation of external-cavity semiconductor lasers with multicavity feedback points as

$$\frac{dS}{dt} = \left(g(n,S) - \frac{1}{\tau_p}\right)S + Q + 2k_c\sqrt{S_\tau(t)S(t)} \times \cos\left[\varphi(t) - \varphi_\tau(t)\right] + F_s(t), \tag{1}$$

$$\frac{d\varphi}{dt} = \frac{1}{2}\alpha G(n - n_{\text{th}}) - k_c\sqrt{\frac{S_\tau(t)}{S(t)}} \times \sin\left[\varphi(t) - \varphi_\tau(t)\right] + F_\varphi(t), \tag{2}$$

$$\frac{dn}{dt} = \frac{I}{e} - \frac{n}{\tau_s} - g(n,S)S + F_n(t), \tag{3}$$

where S, φ, and n are the photon number, photon detuned phase, and carrier number in the main laser cavity, respectively. τ_p is the photon lifetime, τ_s is the carrier lifetime, α is the linewidth-enhancement factor, n_{th} is the number of carriers without feedback and the spontaneous emission, I is the pump current, and e is the electron charge. $\sqrt{S_\tau(t)}$ is the modulus of the total feedback complex electric field, and $S_\tau(t)$ is the total feedback intensity. $\varphi_\tau(t)$ is the detuned phase of the total feedback complex electric field. The slowly varying envelope of the total feedback complex electric field, which is denoted by $\tilde{A}(t)$, i.e., $\tilde{A}(\text{t}) = \sqrt{S_\tau(t)}\exp[-\text{j}\varphi_\tau(t)]$, can be expressed as

$$\tilde{A}(t) = \sum_{i=1}^{N}\sqrt{\frac{S(t-\tau_i)}{N}}\exp\left[-j\varphi(t-\tau_i) - j\omega_0\tau_i\right], \tag{4}$$

where N is the quantity of feedback points, $S(t-\tau_i)$ is the light intensity from each feedback point with the ordinal number of i and the round-trip delay time of τ_i, ω_0 is the center frequency of the semiconductor main-cavity laser without feedback, and $\varphi(t-\tau_i)$ is the light-detuned phase from each feedback point. F_s, F_φ, and F_n are the Langevin noise with Gaussian distribution simulated by random number [59]. k_c is the reflection coefficient of the semiconductor laser, which can be expressed as

$$k_c = \frac{1}{\tau_d}\frac{1-R2}{\sqrt{R2}}\sqrt{f_{\text{ext}}}, \tag{5}$$

where R_2 is the reflection coefficient of the right output mirror of the semiconductor laser main cavity, f_{ext} is the total feedback power fraction of light returned to the main cavity, $\tau_d = 2\eta L_d/c$ is the round-trip time of the main cavity of the laser, η is the refractive index of the laser main cavity, L_d is the length of the main cavity, and c is the speed of light in vacuum. The spontaneous emissivity Q can be expressed as

$$Q = \frac{n_{sp}}{\tau_p}\left(\frac{(\sqrt{R_1}+\sqrt{R_2})(1-\sqrt{R_1R_2})}{\sqrt{R_1R_2}\ln\left(\frac{1}{R_1R_2}\right)}\right)^2, \tag{6}$$

where n_{sp} is the inversion coefficient of semiconductor laser; R_1 and R_2 are the reflection coefficients of the left mirror and the right output mirror of the semiconductor laser main cavity, respectively; and $g(n, S)$ denotes the gain coefficient, which can be expressed as

$$g(n,S) = \frac{G(n-n_0)}{\left(1+\frac{S}{S_0}\right)}, \tag{7}$$

where S_0 corresponds to the photon number with saturation gain, $G(n-n_0)$ is the differential gain, and n_0 is the number of carriers corresponding to zero amplification. The above parameters describe the classical external-cavity semiconductor laser and simulation values are listed in Table I.

TABLE I. Laser parameters.

Symbol	Quantity	Value
L_d	Semiconductor cavity length	1000 μm
I	Pump current	100 mA
η	Semiconductor cavity refractive index	3.6
R_1, R_2	Semiconductor laser mirror reflection	0.32
τ_s	Carrier lifetime	2 ns
τ_p	Photon lifetime	20 ps
n_0	Carrier number to reach zero again	2×10^8
G	$(= v_g dg/dn)$	8×10^{-2} s^{-1}
n_{sp}	Inversion factor	3
A	Linewidth-enhancement factor	3
n_{th}	Carrier number without feedback	5×10^8
S_0	Photon number with saturation gain	5×10^4

We utilize the fourth-order Runge-Kutta method to conduct numerical simulations of the rate equation for the adaptive distributed-feedback semiconductor laser. The Fourier transform is employed to reconstruct the laser spectrum based on the obtained photon number, phase, and carrier number.

Figures 2(b) and 2(e) show the calculated SMSR and intrinsic linewidth of adaptive distributed-feedback semiconductor lasers with different quantity of external-cavity feedback points, each averaged over 10 times. The feedback length of the farthest feedback point is fixed to be 10 m, while the feedback lengths of the other feedback points are randomly distributed within the range from 0 to 10 m. With the total feedback ratio remaining constant to be f_{ext}, the feedback strength of each feedback point is set to be f_{ext}/N when the quantity of feedback points is increased. It can be seen that with increment of the quantity of external-cavity feedback points, the SMSR can be significantly increased by tens of decibels, and the intrinsic linewidth can be narrowed by several times. When the quantity of feedback points reaches around 10, both the SMSR and intrinsic linewidth are gradually stabilized within a certain range. It is worth noting that similar improvement of laser performance on SMSR and linewidth can be obtained under different feedback ratios of 1×10^{-2}, 1×10^{-3} and 1×10^{-4}, respectively, when increasing the quantity of feedback points. The reconstructed spectra of single external-cavity feedback and distributed feedback are shown in Figs. 2(a) and 2(c). With a feedback ratio of 1×10^{-2} and feedback quantity of 200, the SMSR can be significantly enhanced from 15 to 72 dB, compared with the single external-cavity feedback. Similarly, with feedback ratios of 1×10^{-3} and 1×10^{-4}, the SMSR enhancements reaches 37 dB and 27 dB, respectively. The frequency noises of single external-cavity feedback and distributed feedback are shown in Figs. 2(d) and 2(f), respectively. Under distributed feedback, the frequency-noise background below 10^7 Hz band can be reduced by several times, which compresses the intrinsic linewidth. Meanwhile, the frequency-noise peaks in the frequency band beyond 10^7 Hz can be significantly suppressed, which ensures that the external-cavity semiconductor laser can operate from multilongitudinal mode state to the single-longitudinal mode state.

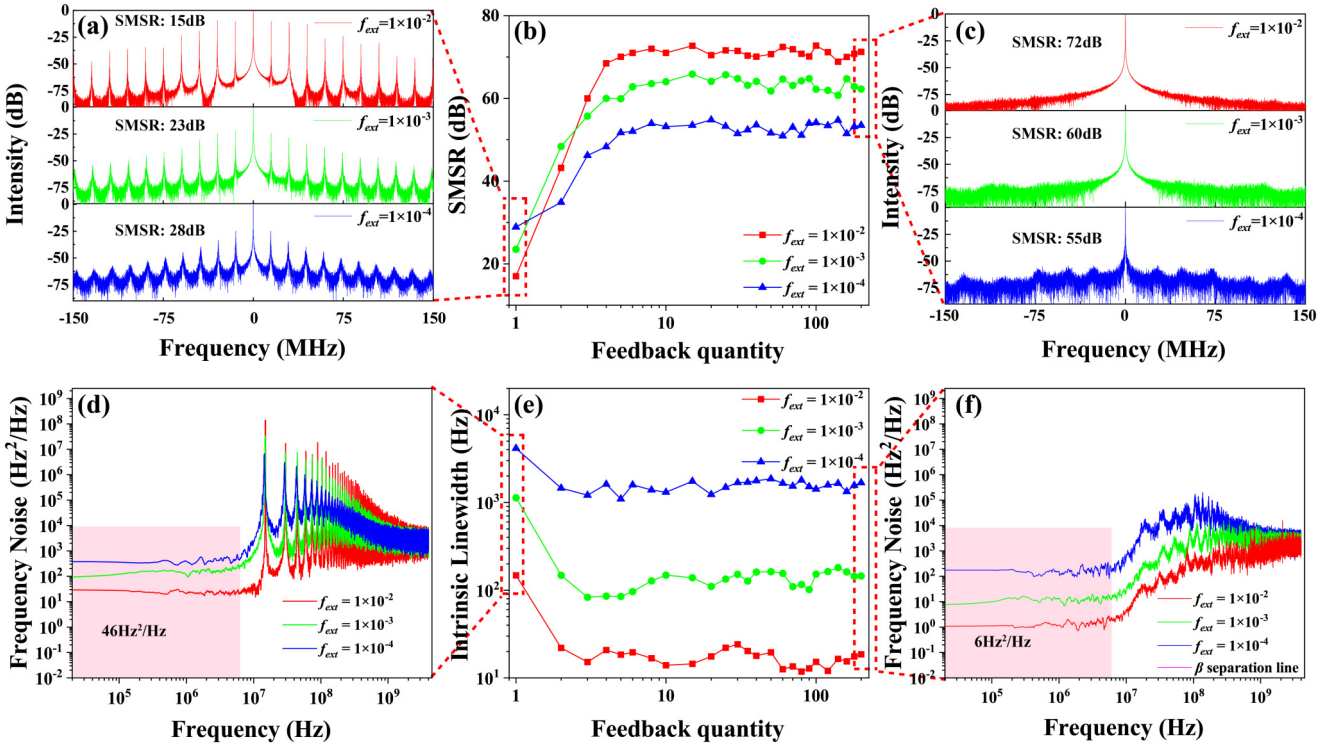

FIG. 2. (a) The reconstructed laser spectra with a single feedback point. (b) The SMSR evolution of external-cavity distributed feedback with different feedback-point quantities. (c) The reconstructed laser spectra with 200 feedback points. (d) Typical frequency noise with a single feedback point. (e) The intrinsic linewidth evolution of external-cavity distributed feedback with different feedback-point quantities. (f) Typical frequency noise with 200 feedback points.

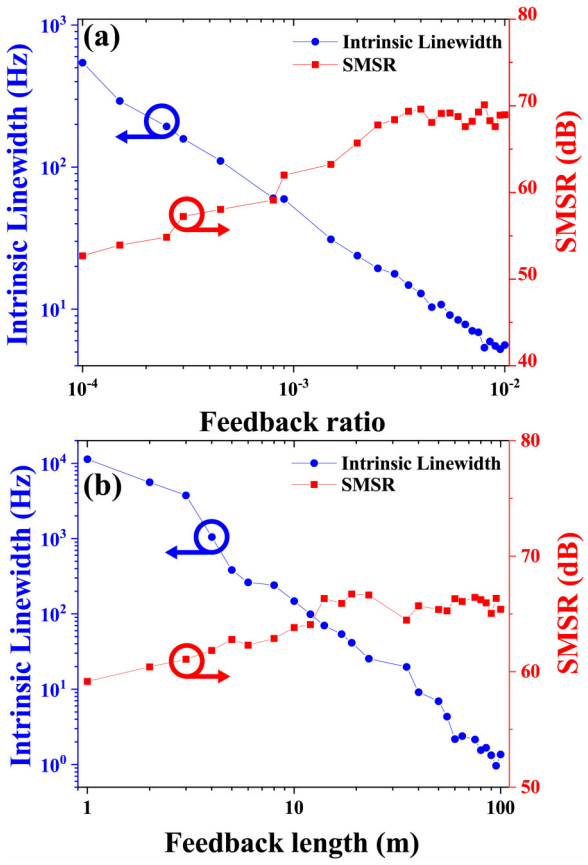

FIG. 3. (a) The SMSR and intrinsic linewidth under different feedback ratios. (b) The SMSR and intrinsic linewidth with different feedback lengths.

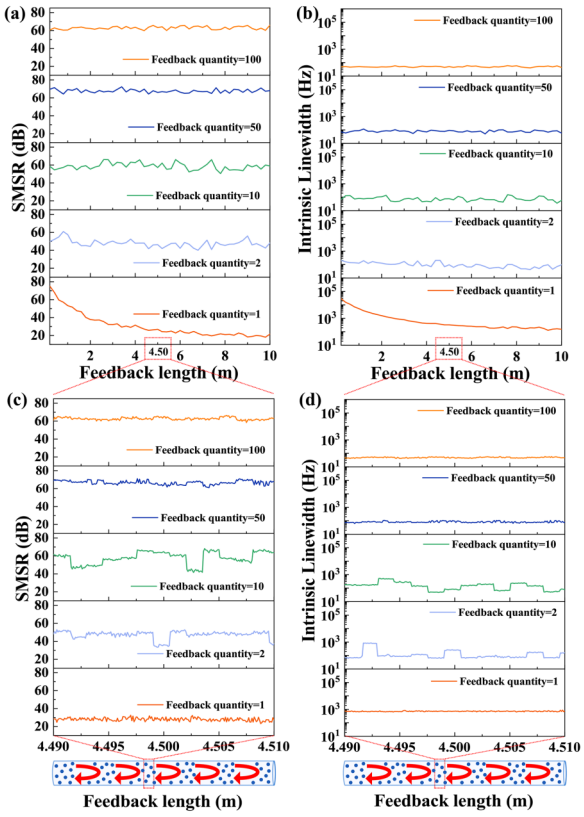

FIG. 4. (a) The SMSR and (b) intrinsic linewidth variations, when changing the feedback length of a specific feedback point and maintaining the feedback length and ratio fixed of other feedback points. (c) The SMSR and (d) intrinsic linewidth variations, by fine changing the specific feedback length from 4.49 to 4.51 m.

On the basis of single-longitudinal mode operation with laser compression by external-cavity distributed feedback, the impact of the feedback ratio and the external-cavity length are further explored to obtain the ultimate SMSR and intrinsic linewidth compression. Figure 3(a) shows the SMSR and intrinsic linewidth under different feedback ratios, with a constant feedback point quantity of 100 and the external-cavity length of 10 m. With the feedback ratio increased from 1×10^{-4} to 1×10^{-2}, the SMSR can be increased from 52 to 70 dB, and the intrinsic linewidth can be compressed from 100-Hz level to 1-Hz level. Similarly, Fig. 3(b) shows the influence of external-cavity length, with a fixed feedback ratio of 1×10^{-3} and the feedback-point quantity of 100. By increasing the external-cavity length, there is a moderate rise in SMSR and a significant compression of intrinsic linewidth. It is worth noting that when the external-cavity length exceeds 10 m and the feedback ratio surpasses 4×10^{-3}, the SMSR approaches a limit while the linewidth can be continuously compressed.

The influence of feedback-point position on the laser linewidth compression is further explored, as shown in Fig. 4. In the simulation, we change the feedback length of a specific feedback point in the distributed-feedback structure while keeping the positions and feedback ratios of other feedback points fixed. Figure 4(a) shows the variation of SMSR when the feedback length of the specific feedback point changes from 0.2 to 10 m. It can be seen that under the condition of single-cavity feedback, the SMSR gradually decreases when increasing the feedback length, as denoted by the red curve. This is due to the longer feedback length bringing more side-longitudinal modes in the single external cavity. Under the condition of dual-feedback points, variation of the feedback length of a specific feedback point can cause severe oscillations of the SMSR, as denoted by the blue curve. When the quantity of the feedback points is increased to 10, there still exists a significant oscillation of the SMSR, as denoted by the green curve. When the quantity of the feedback points is further increased to 50, oscillation of the SMSR tends to weaken. When the quantity of the feedback points is increased to 100, the SMSR is no longer sensitive to the length of a specific feedback point. Due to limitations in simulation computing capabilities, the quantity of different feedback lengths in Fig. 4 is set up to the order of 100, and the adjacent length interval in the x axis of Fig. 4(a) is set to be 0.2 m. In order to improve the accuracy of length calculation, we refine the feedback length variation between 4.49 and 4.51 m with a length accuracy of 0.1 mm around the feedback length of 4.5 m, as shown in Fig. 4(c). The above results indicate that when the quantity of feedback points is increased to dozens, the SMSR can maintain a relatively stable state and is not significantly affected by the specific position fluctuations of specific feedback points. At the same time, we also calculate

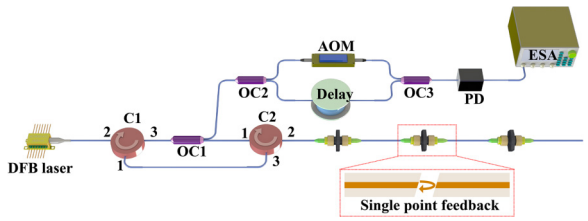

FIG. 5. Experimental setup of the distributed feedback scheme of DFB laser.

the variation in laser intrinsic linewidth when the length of a specific feedback point changes, as shown in Figs. 4(b) and 4(d). Similarly, after the total quantity of feedback points reaches dozens, the laser linewidth can also remain stable and is no longer significantly affected by fluctuations in the position of a specific feedback point. Therefore, by increasing the total quantity of feedback points, the SMSR and linewidth stability of the external-cavity feedback laser can be greatly improved, which will not be affected by the specific position fluctuations of the feedback points. This stable state is applicable to the main-cavity laser working at any wavelength, which achieves the capability of adaptive linewidth compression.

III. EXPERIMENTAL SETUP

To demonstrate the adaptive feature of the proposed external-cavity distributed-feedback laser, we construct an experimental system which utilizes the feedback from the end face of a fiber-optic connector, as shown in Fig. 5. The output of the distributed-feedback (DFB) semiconductor main-cavity laser transmits through a circulator (C1) and an optical coupler (OC1), where 80% of the output laser enters the external-cavity distributed-feedback structure that comprises reflective end faces of multiple fiber-optic connectors, and the feedback light is collected by the other circulator (C2). Before entering the external-cavity distributed-feedback structure, the initial round-trip length between the laser main cavity and port 2 of the circulator C2 is 12 m. The 20% output port of the coupler OC1 is connected to the delayed self-heterodyne interferometry (DSHI) linewidth-measurement system, which consists of two 3-dB couplers (OC2 and OC3), an acousto-optic modulator with a frequency shift of 100 MHz, a fiber delay line, a photodetector, and an electrical spectrum analyzer.

IV. EXPERIMENTAL RESULTS AND DISCUSSION

Figure 6(a) shows intrinsic linewidth variation of the external-cavity semiconductor laser when increasing the distributed-feedback points by connecting multiple fiber-optic connectors. In the experiment, we sequentially increase the quantity of the fiber-optic connectors at port 2 of the circulator C2, which will simultaneously increase the total feedback length and feedback ratio. The box in Fig. 6(a) shows the distance between each feedback point and port 2 of the circulator C2, as well as the accumulated total feedback ratio up to each feedback point. The intrinsic linewidth is compressed from near-10^5-Hz level to 10^2-Hz level with increment of the quantity of the distributed-feedback points. Typical frequency noises in the compression process are shown in Fig. 6(b). The white frequency noise floor is 2.53×10^4 $\mathrm{Hz}^2/\mathrm{Hz}$ and the integrated linewidth is 260.27 kHz, before compression by the distributed-feedback structure, as denoted by the red curve,

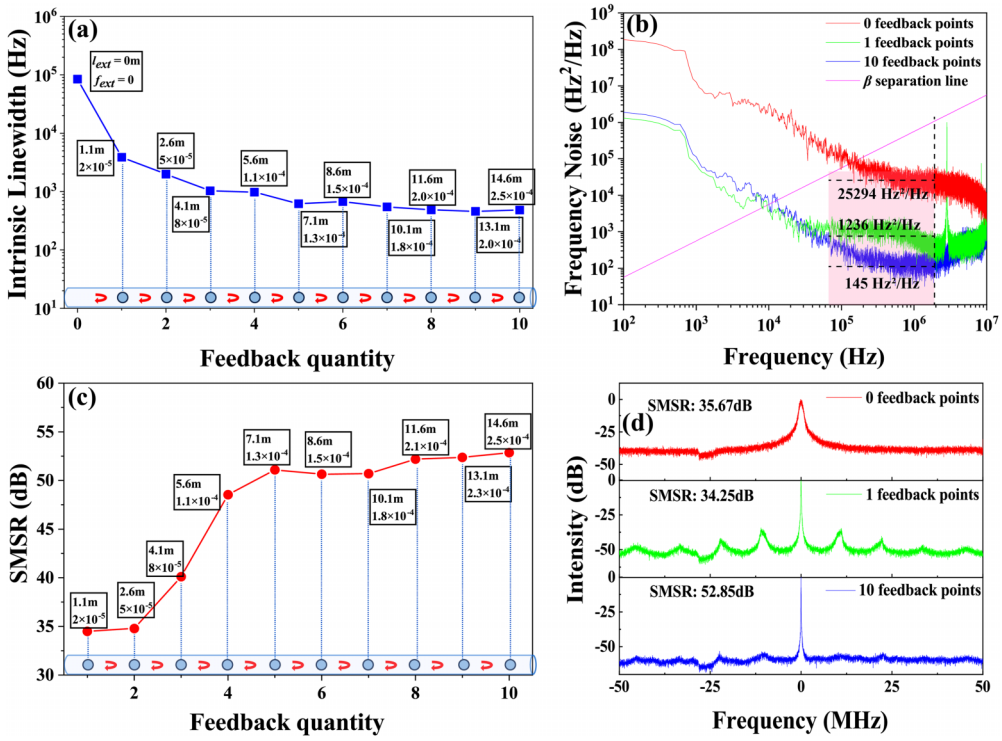

FIG. 6. Experimental demonstration of the external-cavity adaptive distributed-feedback semiconductor laser. (a) Intrinsic linewidth, (b) frequency noise, (c) SMSR, and (d) DSHI spectrum evolution with different feedback-point quantity.

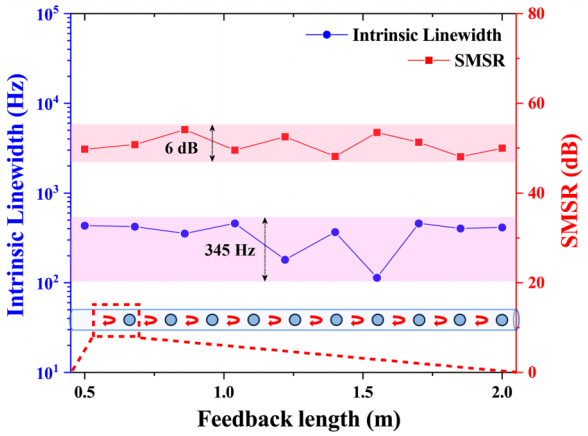

FIG. 7. Adaptability demonstration of the external-cavity distributed feedback by the stability of SMSR and intrinsic linewidth when tuning the feedback length.

which corresponds to an intrinsic linewidth of $\pi \times 2.53 \times 10^4$ $\mathrm{Hz}^2/\mathrm{Hz} = 79.4\,\mathrm{kHz}$. With the single-cavity feedback from the first feedback point, the white frequency noise floor is compressed to be 1.24×10^3 $\mathrm{Hz}^2/\mathrm{Hz}$, with an intrinsic linewidth of $\pi \times 1.24 \times 10^3$ $\mathrm{Hz}^2/\mathrm{Hz} = 3.89\,\mathrm{kHz}$ and an integrated linewidth of 16.98 kHz, as denoted by the green curve. Further increasing the feedback quantity to 10, the white frequency noise floor is compressed to be 145 $\mathrm{Hz}^2/\mathrm{Hz}$, with an intrinsic linewidth of $\pi \times 145$ $\mathrm{Hz}^2/\mathrm{Hz} = 455\,\mathrm{Hz}$ and an integrated linewidth of 20.12 kHz, as denoted by the blue curve. Considering that each fiber-optic connector introduces an insertion loss of 0.5–1 dB, further increasing feedback-point quantity gradually leads to saturated linewidth compression in the experiment. This is due to the accumulated insertion loss of multiple connectors, and the linewidth compression ability of subsequent feedback points gradually decreases. In the meantime, by increasing the quantity of feedback points, the SMSR will be significantly increased from 34.25 to 52.85 dB, as shown in Fig. 6(c). The corresponding DSHI spectrum is shown in Fig. 6(d), where the delayed fiber length in the experiment is 50 km. It can be seen that the single-point feedback introduces strong side-longitudinal modes when compressing the laser linewidth, which is not conducive to single-longitudinal mode operation of the external-cavity feedback laser, as denoted by the green curve. When the quantity of feedback points is increased to 10, all the side-longitudinal modes from the feedback cavity are deeply suppressed, achieving an ultranarrow-linewidth laser in an ideal high-SMSR single-longitudinal mode operation state.

The fiber length between the feedback point and the laser main cavity is further tuned to explore the adaptability of laser linewidth compression with distributed feedback from the external cavity. In the experiment, by gradually reducing the fiber length before the first fiber-optic connector, the distance between all feedback points and the main cavity can be changed simultaneously. When the selected fiber length gradually decreases from 2 to 0.5 m, the SMSR of the adaptive distributed-feedback laser can be maintained at around 50 dB, and the intrinsic linewidth remains in a deep compression state below 1 kHz, as shown in Fig. 7. The experimental results demonstrate that the SMSR and linewidth stability of the external-cavity laser with distributed feedback can be greatly improved, which achieves the capability of adaptive linewidth compression. The adaptability of the external-cavity distributed-feedback laser is not dependent on the specific position of the feedback points, which should also be applicable to different laser wavelengths, due to the wide spectrum characteristics of distributed feedback. The experimental results show that just 10 feedback points have already been enough for adaptive linewidth compression, which is much fewer than the required feedback-point quantity by theoretical prediction that needs more than 50.

V. CONCLUSION

In summary, we propose a theoretical model for analyzing the operation mechanism of adaptive distributed-feedback semiconductor lasers. The influences of the feedback ratio, feedback length, and feedback-point quantity on the performance of adaptive distributed-feedback semiconductor lasers are theoretically and experimentally explored. The results show that increasing the quantity of distributed-feedback points is beneficial for linewidth compression and SMSR promotion, which can largely enhance the stability of single-longitudinal mode operation. Tens of distributed feedback points can implement adaptive linewidth compression, and more feedback points will further enhance the stability of the laser. This work provides a model analysis tool for exploring the ideal configuration of adaptive narrow-linewidth semiconductor lasers, which paves the way for designing and manufacturing of high-performance semiconductor lasers.

The data that support the findings of this study are available from the corresponding author upon reasonable request.

ACKNOWLEDGMENTS

This work is supported by the National Natural Science Foundation of China (NSFC) (Grants No. U23A20378, No. 61935007, and No. 62075020), the Chongqing Natural Science Foundation of Innovative Research Groups (Grant No. cstc2020jcyj-cxttX0005), Fundamental Research Funds for the Central Universities (Grant No. 2024CDJYXTD-004), and the National Science Fund for Distinguished Young Scholars (Grant No. 61825501).

DATA AVAILABILITY

The data that support the findings of this study are available from the corresponding author upon reasonable request.

APPENDIX: DERIVATION OF LASER RATE EQUATIONS FOR MULTICAVITY FEEDBACK POINTS

In a typical laser structure, as shown in Fig. 8, assuming the cavity length is L_d, and reflectivities of the front and back facets R_1 and R_2, the fields E_f and E_b propagating forward- and backward directions are written by

$$E_f(z) = E_{0f} \exp\left\{ikz + \tfrac{1}{2}(g-a)z\right\}, \tag{A1}$$

$$E_b(z) = E_{0b} \exp\left\{ik(L_d - z) + \tfrac{1}{2}(g-a)(L_d - z)\right\}, \tag{A2}$$

where g is the gain coefficient in the laser medium, and a is the total loss in the medium. All the parameters are defined for the laser intensity, so that a factor of 1/2 is introduced in the

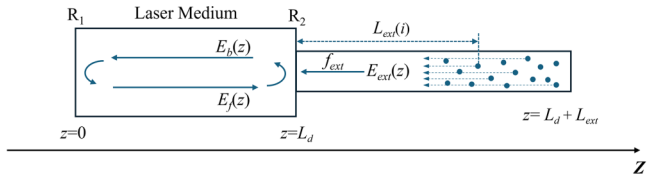

FIG. 8. The Fabry-Pérot resonator with an external feedback cavity, confined between two mirrors by a dielectric medium of length L_d.

above equations. From the boundary conditions at the facets, $E_f(0) = R_1 E_b(0)$ and $E_b(L_d) = R_2 E_f\ (L_d)$, the steady-state condition for the laser oscillation is given by

$$R_1 R_2 \exp\{2ikl + (g-a)L_d\} = 1. \tag{A3}$$

It is convenient to refer to the left-hand side of this condition as the round-trip gain Γ. From threshold onwards $\Gamma = 1$ and all losses are compensated for, while $k = \eta\frac{\omega}{c}$ (where η is the refractive index) must be an integer multiple of π/L_d, which determines the mode frequency. The losses a are considered to be frequency independent, at least for frequencies close to the single-longitudinal mode frequency under consideration [60].

The wavenumber k depends on the refractive index of the laser medium and is a function of the optical frequency ν (or the angular frequency $\omega = 2\pi\nu$) and also the carrier number n. We define the effective refractive index as $\eta_e = \eta + \nu\frac{\partial\eta}{\partial\nu}$. The refractive index of the active layer is a function of the carrier number $n_{\rm th}$ and the optical frequency ν_{th} at the laser threshold and is written by $\eta = \eta_0 + \frac{\partial\eta}{\partial\nu}(\nu - \nu_{th}) + \frac{\partial\eta}{\partial n}(n - n_{th})$ (where η_0 is the refractive index at the threshold). From the relations of $\nu_m = m\frac{c}{2\eta L_d}$ and $\nu_{th} = m\frac{c}{2\eta_0 L_d}$, we assume $\frac{\nu}{\nu_{th}} \approx \frac{\nu_m}{\nu_{th}} = \frac{\eta_0}{\eta} \approx 1$; then, we can obtain $(\nu - \nu_{th}) = -\frac{\nu_{th}}{\eta_e}\frac{\partial\eta}{\partial n}(n - n_{th})$. Therefore, the wavenumber can be expanded by the threshold values of those parameters as

$$k = \eta\frac{\omega}{c} = \frac{\omega_{th}}{c}\left\{\eta_0 + \frac{\partial\eta}{\partial n}(n - n_{th}) + \frac{\eta_e}{\omega_{th}}(\omega - \omega_{th})\right\}. \tag{A4}$$

Using (A4), the round-trip gain Γ can be written by the product of the frequency nondependent and dependent terms, Γ_1 and Γ_2, as

$$\Gamma \equiv \Gamma_1\Gamma_2, \tag{A5}$$

$$\Gamma_1 = R_1 R_2 \exp\{(g-a)L_d + i\phi_0\}, \tag{A6}$$

$$\Gamma_2 = \exp\left\{i\frac{2\omega_{th}L_d}{c}\left[\eta_0 + \frac{\eta_e}{\omega_{th}}(\omega - \omega_{th})\right]\right\}, \tag{A7}$$

The phase ϕ_0 of the above equation is given by

$$\phi_0 = \frac{2\omega_{th}L_d}{c}\frac{\partial\eta}{\partial n}(n - n_{th}) = -\tau_d(\omega - \omega_{th}), \tag{A8}$$

where the cavity round-trip time $\tau_d = \frac{2L_d\eta_e}{c} = \frac{2L_d}{v_g}$(where $v_g = \frac{c}{\eta_e}$ is the group velocity of light in the laser medium).

In (A7), we have used the condition for the laser oscillation that the phase $2\omega_{th}\eta_0 L_d/c$ must be equal to integer multiples of 2π, and therefore irrelevant in the expression for Γ. Then, since the electric field is a sine function, the quantity $-i\omega$ can be replaced with the equivalent to the operator d/dt, and (A7) reads as

$$\Gamma_2 = \exp\{i\tau_d(\omega - \omega_{th})\} = \exp\{-i\omega_{th}\tau_d\}\exp\left\{-\tau_d\frac{d}{dt}\right\}. \tag{A9}$$

To attain the laser oscillations, the complex field after the roundtrip within the laser cavity must coincide exactly with the previous field. Assuming the round-trip gain in between (A5), (A6), and (A8) as a kind of operator, we can obtain the following relation:

$$E_f(t) = \Gamma E_f(t) = \Gamma_1 \exp\{-i\omega_{th}\tau_d\}\exp\left\{-\tau_d\frac{d}{dt}\right\}E_f(t). \tag{A10}$$

Since the laser field will predominantly oscillate at $\omega \approx \omega_{th}$, it is useful to introduce a slowly varying complex amplitude $\tilde{E}(t)$ according to Refs. [61,62]:

$$E_f(t) = \tilde{E}(t)\exp\{-i\omega_{th}t\}. \tag{A11}$$

With this expression and the fact that the operator $\exp(-\tau_d\, d/dt)$ is equivalent to the time-delay effect of τ_d, (A10) yields

$$\tilde{E}(t)\exp\{-i\omega_{th}t\} = \Gamma_1\exp\{-i\omega_{th}\tau_d\}\tilde{E}(t-\tau_d) \times \exp\{-i\omega_{th}(t-\tau_d)\}. \tag{A12}$$

Therefore, we can write the field $\tilde{E}(t)$ as

$$\tilde{E}(t) = \Gamma_1\tilde{E}(t-\tau_d). \tag{A13}$$

When variations in $\tilde{E}(t)$ during one round-trip time are small, this difference equation can be approximated by a first-order differential equation:

$$\tilde{E}(t-\tau_d) \simeq \tilde{E}(t) - \tau_d\frac{d\tilde{E}(t)}{dt}. \tag{A14}$$

Then, we obtain the differential form for the field as follows:

$$\frac{d\tilde{E}(t)}{dt} = \frac{1}{\tau_d}\left(1 - \frac{1}{\Gamma_1}\right)\tilde{E}(t). \tag{A15}$$

Since the gain Γ_1 is very close to unity for laser oscillation, we approximate the gain from (A6) as

$$\frac{1}{\Gamma_1} = \exp\{-\ln(R_1R_2) - (g-a)L_d - i\phi_0\} \approx 1 + \ln\frac{1}{R_1R_2} - gL_d + aL_d - i\phi_0. \tag{A16}$$

Substituting the above equation into (A15) and using the relation of (A8), we finally obtain the rate equation for the field as

$$\frac{d\tilde{E}(t)}{dt} = \left\{-i(\omega_0 - \omega_{th}) + \frac{1}{2}\left(gv_g - \frac{1}{\tau_p}\right)\right\}\tilde{E}(t), \tag{A17}$$

where τ_p is the photon lifetime and the laser is assumed to operate at the angular optical frequency of $\omega = \omega_0$.

With the definition of linewidth enhancement factor $\alpha = -2\frac{\omega}{c}\frac{\frac{\partial\eta}{\partial n}}{\frac{\partial g}{\partial n}}$ together with $(\nu - \nu_{th}) = -\frac{\nu_{th}}{\eta_e}\frac{\partial\eta}{\partial n}(n - n_{th})$, we have

$$(\omega - \omega_{th}) = -\frac{1}{2}\alpha v_g\frac{\partial g}{\partial n}(n - n_{th}). \tag{A18}$$

Then, the field equation is a function of the time-dependent carrier number and it is rewritten as

$$\frac{d\tilde{E}(t)}{dt} = \frac{1}{2}(1 - i\alpha)G[n(t) - n_{th}]\tilde{E}(t), \tag{A19}$$

where $G = v_g \partial g/\partial n$ is the linear gain. Finally, considering the effect of spontaneous emissions of light and statistical Langevin noises in laser oscillations, we obtain the field equation as

$$\frac{d\tilde{E}(t)}{dt} = \frac{1}{2}(1 - i\alpha)G[n(t) - n_{th}]\tilde{E}(t) + \tilde{E}_{sp}(t) + \tilde{F}_E(t), \tag{A20}$$

where F_E(t) is a Langevin force describing a (Gaussian) white-noise process. We assume that the noise is like a shot noise, the correlation time is short enough, and Langevin forces satisfy the general relations [63]

$$\langle F_i(t)\rangle = 0, \tag{A21}$$

$$\langle F_i(t)F_j(t')\rangle = 2D_{ij}\delta(t - t'), \tag{A22}$$

where D_{ij} is the diffusion coefficient for the differential diffusion equation in the presence of the Langevin force.

The case of external optical feedback from an total external power reflectivity f_{ext} can be treated in a similar way. The amplitude E_b of the wave traveling in the negative-z direction at $z = 0$ is the result of both the reflection of E_f and the entering of the amplitude of the wave inside the external cavity. Due to the weak distributed feedback with extremely low reflectivity at each point, the feedback can be approximated by taking into account just one external roundtrip:

$$\begin{aligned} E_b(t) &= \sqrt{R_2}E_f(t) + (1 - R_2)E_{\tau_1}(t - \tau_1)\exp\{-i\omega_{th}\tau_1\} \\ &\quad + (1 - R_2)E_{\tau_2}(t - \tau_2)\exp\{-i\omega_{th}\tau_2\} + (1 - R_2) \\ &\quad \times E_{\tau_3}(t - \tau_3)\exp\{-i\omega_{th}\tau_3\} + ... \\ &= \sqrt{R_2}[E_f(t) + E_{\text{ext}}(t)]. \end{aligned} \tag{A23}$$

The external signal E_{ext} can thus be written as

$$E_{\text{ext}}(t) = \frac{1 - R_2}{\sqrt{R_2}}\sum_{m=1}^{N} E_{\tau_m}(t - \tau_m)\exp\{-i\omega_{th}\tau_m\}. \tag{A24}$$

Similar to (A13)–(A15), we can obtain

$$\tilde{E}(t + \tau_d) = \Gamma_1[\tilde{E}(t) + \tilde{E}_{\text{ext}}(t)], \tag{A25}$$

$$\frac{d\tilde{E}(t)}{dt} = \frac{1}{\tau_d}(\Gamma_1 - 1)\tilde{E}(t) + \frac{1}{\tau_d}\Gamma_1\tilde{E}_{\text{ext}}(t). \tag{A26}$$

By introducing (A16) and considering $\Gamma_1 \approx 1$ during laser oscillation, we can obtain a similar result:

$$\begin{aligned} \frac{d\tilde{E}(t)}{dt} &= \frac{1}{2}(1 + i\alpha)G[n(t) - n_{th}]\tilde{E}(t) + \tilde{E}_{\text{ext}} + \tilde{E}_{sp}(t) + \tilde{F}_E(t) \\ &= \frac{1}{2}(1 + i\alpha)G[n(t) - n_{th}]\tilde{E}(t) + \frac{1}{\tau_d}\frac{1 - R_2}{\sqrt{R_2}} \\ &\quad \times \sum_{m=1}^{N}\tilde{E}_{\tau_m}(t - \tau_m)\exp\{-i\omega_{th}\tau_m\} + \tilde{E}_{sp}(t) + \tilde{F}_E(t). \end{aligned} \tag{A27}$$

Since the feedback from multiple points in the external cavity ultimately enters into the main cavity, in this model we represent the feedback photon flux in the external cavity as a single beam, where the feedback energy entering the main cavity is determined by the coefficient f_{ext}. Using the notation of the complex field $\tilde{E}(t) = \sqrt{S(t)}\exp\{-i\varphi(t)\}$, the total electric field of the external cavity can be written as

$$\begin{aligned} \frac{1 - R_2}{\sqrt{R_2}}\sum_{m=1}^{\infty}\tilde{E}_{\tau_m}(t - \tau_m)\exp\{-i\omega_{th}\tau_m\} &= \frac{1 - R_2}{\sqrt{R_2}}\sqrt{f_{\text{ext}}}\sum_{m=1}^{N}\sqrt{\frac{S(t - \tau_m)}{N}}\exp[-i\varphi(t - \tau_m)]\exp\{-i\omega_{th}\tau_m\} \\ &= \frac{1 - R_2}{\sqrt{R_2}}\sqrt{f_{\text{ext}}}\sqrt{S_\tau(t)}\exp[-i\varphi_\tau(t)]. \end{aligned} \tag{A28}$$

Then, the photon number $S(t) = |\tilde{E}(t)|^2$ and the phase $\varphi(t)$ of the field equation are separately given by

$$\begin{aligned} \frac{dS}{dt} &= \tilde{E}(t)\frac{d\tilde{E}^*(t)}{dt} + \tilde{E}^*(t)\frac{d\tilde{E}(t)}{dt} = 2\text{Re}\left[\tilde{E}^*(t)\frac{d\tilde{E}(t)}{dt}\right] \\ &= G[n(t) - n_{th}]S + 2\text{Re}\left[\tilde{E}^*(t)\frac{1}{\tau_d}\frac{1 - R_2}{\sqrt{R_2}}\sqrt{f_{\text{ext}}}\sqrt{S_\tau(t)}\exp[-i\varphi_\tau(t)]\right] + 2\text{Re}[\tilde{E}^*(t)\tilde{E}_{sp}(t)] + F_S(t) \\ &= \left(g(n) - \frac{1}{\tau_p}\right)S + 2k_c\sqrt{S_\tau(t)S(t)}\cos[\varphi(t) - \varphi_\tau(t)] + 2\text{Re}\left[\tilde{E}^*(t)\tilde{E}_{sp}(t)\right] + F_S(t), \end{aligned} \tag{A29}$$

$$\begin{aligned} \frac{d\varphi}{dt} &= \frac{1}{S(t)}\text{Im}\left[\tilde{E}^*(t)\frac{d\tilde{E}(t)}{dt}\right] \\ &= \frac{1}{2}\alpha G(n - n_{th}) - k_c\sqrt{\frac{S_\tau(t)}{S(t)}}\sin[\varphi(t) - \varphi_\tau(t)] + F_\varphi(t), \end{aligned} \tag{A30}$$

where $k_c = \frac{1}{\tau_d}\frac{1-R_2}{\sqrt{R_2}}\sqrt{f_{\text{ext}}}$ is defined as the reflection coefficient; $g(n)$ is the linear gain in medium and defined as $g(n) = \frac{\partial g}{\partial n}(n_{th} - n_0) + \frac{\partial g}{\partial n}(n - n_{th}) = g_{th}(n) + G(n - n_{th})$. The $g_{th}(n)$ is the gain of the medium at the threshold; therefore, we know that $g_{th}(n) = \frac{1}{\tau_p}$.

Equations (A29) and (A30) represent the time evolution of the photon number and the phase of the slave laser. For the numerical simulation, two extensions have been made:

1. An eventual multimode emission of the master and slave laser is taken into account.
2. Nonlinear gain is considered.

Nonlinear gain may be introduced either by intrinsic nonlinearities of the laser medium or by an effective nonlinearity due to diffusion effects. In this model, we will assume equal nonlinear gain suppression for all modes, which corresponds to the diffusion model in Ref. [64]. The gain is then expressed as

$$g(n, S) = \frac{G(n - n_0)}{\left(1 + \frac{S}{S_0}\right)}, \tag{A31}$$

where S_0 corresponds to the photon number with saturation gain.

Thus, the rate equations can be rewritten as

$$\frac{dS}{dt} = \left(g(n, S) - \frac{1}{\tau_p}\right)S + 2k_c\sqrt{S_\tau(t)S(t)}$$
$$\cos[\varphi(t) - \varphi_\tau(t)] + 2\text{Re}[\tilde{E}^*(t)\tilde{E}_{sp}(t)] + F_S(t), \tag{A32}$$

$$\frac{d\varphi}{dt} = \frac{1}{2}\alpha G(n - n_{th}) - k_c\sqrt{\frac{S_\tau(t)}{S(t)}}$$
$$\sin[\varphi(t) - \varphi_\tau(t)] + F_\varphi(t). \tag{A33}$$

We define the spontaneous emission term as Q and consider the laser cavity as a Fabry-Pérot cavity [65]. We can obtain

$$2\text{Re}[\tilde{E}^*(t)\tilde{E}_{sp}(t)] = Q = \frac{n_{sp}}{\tau_p}\left(\frac{(\sqrt{R_1} + \sqrt{R_2})(1 - \sqrt{R_1R_2})}{\sqrt{R_1R_2}\ln\left(\frac{1}{R_1R_2}\right)}\right)^2, \tag{A34}$$

where n_{sp} is the inversion factor.

As we know, the carrier number n is mainly composed of carrier production term $\frac{I}{e}$, spontaneous recombination $-\frac{n}{\tau_s}$, the stimulated recombination rate $-g(n, S)S$, and Langevin noises $F_n(t)$. Therefore, the rate equation for the number of charge carriers can be obtained:

$$\frac{dn}{dt} = \frac{I}{e} - \frac{n}{\tau_s} - g(n, S)S + F_n(t), \tag{A35}$$

where I is the pump current, e is the electron charge, and τ_s is the carrier lifetime.

Thus, we can get the laser rate equation of multicavity feedback-point semiconductor lasers:

$$\frac{dS}{dt} = \left(g(n, S) - \frac{1}{\tau_p}\right)S + Q + 2k_c\sqrt{S_\tau(t)S(t)}$$
$$\cos[\varphi(t) - \varphi_\tau(t)] + F_S(t), \tag{A36}$$

$$\frac{d\varphi}{dt} = \frac{1}{2}\alpha G(n - n_{th}) - k_c\sqrt{\frac{S_\tau(t)}{S(t)}}\sin[\varphi(t) - \varphi_\tau(t)] + F_\varphi(t), \tag{A37}$$

$$\frac{dn}{dt} = \frac{I}{e} - \frac{n}{\tau_s} - g(n, S)S + F_n(t). \tag{A38}$$

[1] L. S. Froufe-Pérez, W. Gueri, R. Carminati, and R. Kaiser, Threshold of a random laser with cold atoms, Phys. Rev. Lett. **102**, 173903 (2009).

[2] Q. Baudouin, N. Mercadier, V. Guarrera, W. Guerin, and R. Kaiser, A cold-atom random laser, Nat. Phys. **9**, 357 (2013).

[3] L. Liu, D. Lü, W. Chen, T. Li, Q. Qu, B. Wang, L. Li, W. Ren, Z. Dong, J. Zhao, W. Xia, X. Zhao, J. Ji, M. Ye, Y. Sun, Y. Yao, D. Song, Z. Liang, S. Hu, D. Yu *et al.*, In-orbit operation of an atomic clock based on laser-cooled 87 Rb atoms, Nat. Commun. **9**, 2760 (2018).

[4] W. Loh, J. Stuart, D. Reens, C. D. Bruzewicz, D. Braje, J. Chiaverini, P. W. Juodawlkis, J. M. Sage, and R. McConnell, Operation of an optical atomic clock with a Brillouin laser subsystem, Nature (London) **588**, 244 (2020).

[5] R. Lange, N. Huntemann, J. M. Rahm, C. Sanner, H. Shao, B. Lipphardt, C. Tamm, S. Weyers, and E. Peik, Improved limits for violations of local position invariance from atomic clock comparisons, Phys. Rev. Lett. **126**, 011102 (2021).

[6] P. W. Graham, J. M. Hogan, M. A. Kasevich, and S. Rajendran, New method for gravitational wave detection with atomic sensors, Phys. Rev. Lett. **110**, 171102 (2013).

[7] A. Arvanitaki and A. A. Geraci, Detecting high-frequency gravitational waves with optically levitated sensors, Phys. Rev. Lett. **110**, 071105 (2013).

[8] B. P. Abbott, R. Abbott, T. D. Abbott, M. R. Abernathy, F. Acernese, K. Ackley, C. Adams, T. Adams, P. Addesso *et al.* (LIGO Scientific Collaboration and Virgo Collaboration), Observation of gravitational waves from a binary black hole merger, Phys. Rev. Lett. **116**, 061102 (2016).

[9] N. Aggarwal, G. P. Winstone, M. Teo, M. Baryakhtar, S. L. Larson, V. Kalogera, and A. A. Geraci, Searching for new physics with a levitated-sensor-based gravitational-wave detector, Phys. Rev. Lett. **128**, 111101 (2022).

[10] F. Meylahn, B. Willke, and H. Vahlbruch, Squeezed states of light for future gravitational wave detectors at a wavelength of 1550 nm, Phys. Rev. Lett. **129**, 121103 (2022).

[11] R. Bouchendira, P. Cladé, S. Guellati-Khélifa, F. Nez, and F. Biraben, New determination of the fine structure constant and test of the quantum electrodynamics, Phys. Rev. Lett. **106**, 080801 (2011).

[12] S. Haroche, M. Brune, and J. M. Raimond, From cavity to circuit quantum electrodynamics, Nat. Phys. **16**, 243 (2020).

[13] M. Lei, R. Fukumori, J. Rochman, B. Zhu, M. Endres, J. Choi, and A. Faraon, Many-body cavity quantum electrodynamics with driven inhomogeneous emitters, Nature (London) **617**, 271 (2023).

[14] P. Steindl, J. A. Frey, J. Norman, J. E. Bowers, D. Bouwmeester, and W. Löffler, Cross-polarization-extinction enhancement and spin-orbit coupling of light for quantum-dot cavity quantum electrodynamics spectroscopy, Phys. Rev. Appl. **19**, 064082 (2023).

[15] P. Marin-Palomo, J. N. Kemal, M. Karpov, A. Kordts, J. Pfeifle, M. H. P. Pfeiffer, P. Trocha, S. Wolf, V. Brasch, M. H. Anderson, R. Rosenberger, K. Vijayan, W. Freude, T. J. Kippenberg, and C. Koos, Microresonator-based solitons for massively parallel coherent optical communications, Nature (London) **546**, 274 (2017).

[16] Y. Geng, H. Zhou, X. Han, W. Cui, Q. Zhang, B. Liu, G. Deng, Q. Zhou, and K. Qiu, Coherent optical communications using coherence-cloned Kerr soliton microcombs, Nat. Commun. **13**, 1070 (2022).

[17] D. J. Jones, S. A. Diddams, J. K. Ranka, A. Stentz, R. S. Windeler, J. L. Hall, and S. T. Cundiff, Carrier-envelope phase control of femtosecond mode-locked lasers and direct optical frequency synthesis, Science **288**, 635 (2000).

[18] M. A. Barrios, D. G. Hicks, T. R. Boehly, D. E. Fratanduono, J. H. Eggert, P. M. Celliers, G. W. Collins, and D. D. Meyerhofer, High-precision measurements of the equation of state of hydrocarbons at 1–10 Mbar using laser-driven shock waves, Phys. Plasmas **17**, 056307 (2010).

[19] F. R. Giorgetta, I. Coddington, E. Baumann, W. C. Swann, and N. R. Newbury, Fast high-resolution spectroscopy of dynamic continuous-wave laser sources, Nat. Photonics **4**, 853 (2010).

[20] B. Dong, Y. Wan, W. W. Chow, C. Shang, A. Prokoshin, E. Alkhazraji, R. Koscica, H. Wang, and J. E. Bowers, Turnkey locking of quantum-dot lasers directly grown on Si, Nat. Photonics **18**, 669 (2024).

[21] S. Wang, Z. Lv, Q. Yang, S. Wang, H. Chai, L. Meng, D. Lu, C. Ji, X.-G. Yang, and T. Yang, High-power, narrow-linewidth, and low-noise quantum dot distributed feedback lasers, Laser Photonics Rev. **17**, 2200979 (2023).

[22] J. H. Surrow, S. T. Thomsen, R. R. Kumar, M. F. Brusatori, M. P. Montes, A. S. Palsole, C. Hoede, H. N. Klein, and N. Volet, Ultra-narrow linewidth laser across the C-band using polarization-controlled dual-cavity feedback, Opt. Express **33**, 11863 (2025).

[23] C. Xiang, J. Guo, W. Jin, L. Wu, J. Peters, W. Xie, L. Chang, B. Shen, H. Wang, Q. Yang, D. Kinghorn, M. Paniccia, K. J. Vahala, P. A. Morton, and J. E. Bowers, High-performance lasers for fully integrated silicon nitride photonics, Nat. Commun. **12**, 6650 (2021).

[24] A. E. Shitikov, I. I. Lykov, O. V. Benderov, D. A. Chermoshentsev, I. K. Gorelov, A. N. Danilin, R. R. Galiev, N. M. Kondratiev, S. J. Cordette, A. V. Rodin, A. V. Masalov, V. E. Lobanov, and I. A. Bilenko, Optimization of laser stabilization via self-injection locking to a whispering-gallery-mode microresonator, Phys. Rev. Appl. **14**, 014036 (2020).

[25] W. Jin, Q. F. Yang, L. Chang, B. Shen, H. Wang, M. A. Leal, L. Wu, M. Gao, A. Feshali, M. Paniccia, K. J. Vahala, and J. E. Bowers, Hertz-linewidth semiconductor lasers using CMOS-ready ultra-high-Q microresonators, Nat. Photonics **15**, 346 (2021).

[26] A. E. Shitikov, R. R. Galiev, K. N. Min'kov, N. M. Kondratiev, S. J. Cordette, V. E. Lobanov, and I. A. Bilenko, Red narrow-linewidth lasing and frequency comb from gain-switched self-injection-locked Fabry–Pérot laser diode, Sci. Rep. **13**, 9830 (2023).

[27] M. A. Tran, C. Zhang, T. J. Morin, L. Chang, S. Barik, Z. Yuan, W. Lee, G. Kim, A. Malik, Z. Zhang, J. Guo, H. Wang, B. Shen, L. Wu, K. Vahala, J. E. Bowers, H. Park, and T. Komljenovic, Extending the spectrum of fully integrated photonics to submicrometre wavelengths, Nature (London) **610**, 54 (2022).

[28] A. Siddharth, T. Wunderer, G. Lihachev, A. S. Voloshin, C. Haller, R. N. Wang, M. Teepe, Z. Yang, J. Liu, J. Riemensberger, N. Grandjean, N. Johnson, and T. J. Kippenberg, Near ultraviolet photonic integrated lasers based on silicon nitride, APL Photonics **7**, 046108 (2022).

[29] B. Li, Z. Yuan, W. Jin, L. Wu, J. Guo, Q. Ji, A. Feshali, M. Paniccia, J. E. Bowers, and K. J. Vahala, High-coherence hybrid-integrated 780 nm source by self-injection-locked second-harmonic generation in a high-Q silicon-nitride resonator, Optica **10**, 1241 (2023).

[30] Z. Zhang, B. Shen, M. A. Tran, W. Lee, K. Asawa, G. Kim, Y. Shen, T. J. Morin, A. Malik, J. E. Bowers, T. Komljenovic, and C. Zhang, Photonic integration platform for rubidium sensors and beyond, Optica **10**, 752 (2023).

[31] A. Prokoshin, M. Gehl, S. Madaras, W. W. Chow, and Y. Wan, Ultra-narrow-linewidth hybrid-integrated self-injection locked laser at 780 nm, Optica **11**, 1024 (2024).

[32] A. Prokoshin, W. W. Chow, B. Dong, F. Grillot, J. Bowers, and Y. Wan, Linewidth narrowing in self-injection locked lasers: Effects of quantum confinement, APL Photonics **9**, 086106 (2024).

[33] E. Alkhazraji, W. W. Chow, F. Grillot, J. E. Bowers, and Y. Wan, Linewidth narrowing in self-injection-locked on-chip lasers, Light Sci. Appl. **12**, 162 (2023).

[34] F. Lei, Z. Ye, Ó. B. Helgason, A. Fülöp, M. Girardi, and V. Torres-Company, Optical linewidth of soliton microcombs, Nat. Commun. **13**, 3161 (2022).

[35] M. Corato-Zanarella, A. Gil-Molina, X. Ji, M. C. Shin, A. Mohanty, and M. Lipson, Widely tunable and narrow-linewidth chip-scale lasers from near-ultraviolet to near-infrared wavelengths, Nat. Photonics **17**, 157 (2023).

[36] T. Zhu, X. Bao, L. Chen, H. Liang, and Y. Dong, Experimental study on stimulated Rayleigh scattering in optical fibers, Opt. Express **18**, 22958 (2010).

[37] T. Zhu, X. Bao, and L. Chen, A single longitudinal-mode tunable fiber ring laser based on stimulated Rayleigh scattering in a nonuniform optical fiber, J. Lightwave Technol. **29**, 1802 (2011).

[38] T. Zhu, Y. F. Chen, S. Huang, and X. Bao, An ultra-narrow linewidth fiber laser based on Rayleigh backscattering in a tapered optical fiber, Laser Phys. Lett. **10**, 055110 (2013).

[39] L. Dang, L. Huang, Y. Cao, Y. Li, P. I. Iroegbu, T. Lan, L. Shi, G. Yin, and T. Zhu, Side mode suppression of SOA fiber hybrid laser based on distributed self-injection feedback, Opt. Laser Technol. **147**, 107619 (2022).

[40] T. Zhu, S. Huang, L. Shi, W. Huang, M. Liu, and K. Chiang, Rayleigh backscattering: A method to highly compress laser linewidth, Chin. Sci. Bull. **59**, 4631 (2014).

[41] T. Zhu, B. Zhang, L. Shi, S. Huang, M. Deng, J. Liu, and X. Li, Tunable dual-wavelength fiber laser with ultra-narrow linewidth based on Rayleigh backscattering, Opt. Express **24**, 1324 (2016).

[42] S. Huang, T. Zhu, G. Yin, S. Huang, M. Deng, J. Liu, and X. Li, Tens of hertz narrow-linewidth laser based on stimulated Brillouin and Rayleigh scattering, Opt. Lett. **42**, 5286 (2017).

[43] Y. Li, L. Huang, L. Gao, T. Lan, Y. Cao, I. P. Ikechukwu, L. Shi, Y. Liu, F. Li, and T. Zhu, Optically controlled tunable ultra-narrow linewidth fiber laser with Rayleigh backscattering and saturable absorption ring, Opt. Express **26**, 26896 (2018).

[44] F. Li, T. Lan, L. Huang, I. P. Ikechukwu, W. Liu, and T. Zhu, Spectrum evolution of Rayleigh backscattering in one-dimensional waveguide, Opto-Electron. Adv. **2**, 190012 (2019).

[45] L. Dang, L. Huang, L. Shi, F. Li, G. Yin, L. Gao, T. Lan, Y. Li, L. Jiang, and T. Zhu, Ultra-high spectral purity laser derived from weak external distributed perturbation, Opto-Electron. Adv. **6**, 210149 (2023).

[46] J. Li, T. Lan, L. Dang, J. Li, L. Huang, L. Shi, G. Yin, and T. Zhu, Ultra-narrow linewidth vertical-cavity surface-emitting laser based on external-cavity weak distributed feedback, Opt. Express **30**, 37519 (2022).

[47] J. Li, J. Luo, L. Shi, D. Wei, L. Jin, T. Liu, and T. Zhu, Rayleigh backscattering-based simultaneous linewidth narrowing of a multi-wavelength DFB laser array with an arbitrary wavelength spacin, Opt. Lett. **48**, 6188 (2023).

[48] A. Consoli and C. López, Decoupling gain and feedback in coherent random lasers: Experiments and simulations, Sci. Rep. **5**, 16848 (2015).

[49] R. Reimann, W. Alt, T. Kampschulte, T. Macha, L. Ratschbacher, N. Thau, S. Yoon, and D. Meschede, Cavity-modified collective Rayleigh scattering of two atoms, Phys. Rev. Lett. **114**, 023601 (2015).

[50] S. A. Babin, E. A. Zlobina, S. I. Kablukov, and E. V. Podivilov, High-order random Raman lasing in a PM fiber with ultimate efficiency and narrow bandwidth, Sci. Rep. **6**, 22625 (2016).

[51] S. Gao, L. Zhang, Y. Xu, P. Lu, L. Chen, and X. Bao, Tapered fiber based Brillouin random fiber laser and its application for linewidth measurement, Opt. Express **24**, 28353 (2016).

[52] I. A. Lobach, S. I. Kablukov, M. I. Skvortsov, E. V. Podivilov, M. A. Melkumov, S. A. Babin, and E. M. Dianov, Narrowband random lasing in a Bismuth-doped active fiber, Sci. Rep. **6**, 30083 (2016).

[53] Y. Xu, L. Zhang, L. Chen, and X. Bao, Single-mode SOA-based 1kHz-linewidth dual-wavelength random fiber laser, Opt. Express **25**, 15828 (2017).

[54] J. Xu, L. Huangm, M. Jiang, J. Ye, P. Ma, J. Leng, J. Wu, H. Zhang, and P. Zhou, Near-diffraction-limited linearly polarized narrow-linewidth random fiber laser with record kilowatt output, Photonics Res. **5**, 350 (2017).

[55] A. Boschetti, A. Taschin, P. Bartolini, A. K. Tiwari, L. Pattelli, R. Torre, and D. S. Wiersma, Spectral super-resolution spectroscopy using a random laser, Nat. Photonics **14**, 177 (2020).

[56] M. I. Skvortsov, A. A. Wolf, A. V. Dostovalov, O. N. Egorova, S. L. Semjonov, and S. A. Babin, Narrow-linewidth Er-doped fiber lasers with random distributed feedback provided by artificial Rayleigh scattering, J. Lightwave Technol. **40**, 1829 (2022).

[57] A. Consoli, N. Caselli, and C. López, Electrically driven random lasing from a modified Fabry–Pérot laser diode, Nat. Photonics **16**, 219 (2022).

[58] N. Schunk and K. Petermann, Noise analysis of injection-locked semiconductor injection lasers, IEEE. J. Quantum Elect. **22**, 642 (1986).

[59] N. Schunk and K. Petermann, Numerical analysis of the feedback regimes for a single-mode semiconductor laser with external feedback, IEEE. J. Quantum Elect. **24**, 1242 (1988).

[60] K. Petermann, *Laser Diode Modulation and Noise* (Kluwer Academic, Dordrecht, 1988).

[61] M. Sargent, M. O. Scully, and W. E. Lamb, *Laser Physics* (Addison-Wesley, Reading, 1974).

[62] H. Haken, *Laser Light Dynamics* (North-Holland Physics Publishing, Amsterdam, 1986).

[63] N. G. van Kampen, *Stochastic Processes in Physics and Chemistry* (North-Holland, Amsterdam, 1981).

[64] R. S. Tucker and D. J. Pope, Circuit modeling of the effect of diffusion on damping in a narrow-stripe semiconductor laser, IEEE J. Quantum Electron. **19**, 1179 (1983).

[65] C. H. Henry, Theory of spontaneous emission noise in open resonators and its application to lasers and optical amplifiers, J. Lightwave Technol. **4**, 288 (1986).